

SiC detector damage and characterization for high intensity laser-plasma diagnostics

This content has been downloaded from IOPscience. Please scroll down to see the full text.

2016 JINST 11 P05009

(<http://iopscience.iop.org/1748-0221/11/05/P05009>)

View [the table of contents for this issue](#), or go to the [journal homepage](#) for more

Download details:

IP Address: 210.72.8.209

This content was downloaded on 30/12/2016 at 05:24

Please note that [terms and conditions apply](#).

You may also be interested in:

[SiC detectors for radiation sources characterization and fast plasma diagnostic](#)

A. Cannavò and L. Torrisi

[Silicon carbide detectors for diagnostics of ion emission from laser plasmas](#)

Paolo Musumeci, Maria Cutroneo, Lorenzo Torrisi et al.

[Active Resonant Antennas for Gravitational Radiation](#)

Hiromasa Hirakawa, Kimio Tsubono and Katsunobu Oide

[Review of amorphous silicon based particle detectors: The quest for single particle detection](#)

N Wyrsh and C Ballif

[SiC detector characterization for radiation emitted by laser-generated plasmas](#)

A. Cannavò, L. Torrisi and L. Calcagno

[Laser-plasma interaction in direct-drive inertial confinement fusion](#)

J F Myatt, J Shaw, V N Goncharov et al.

[Radiation damage effects in Si materials and detectors and rad-hard Si detectors for SLHC](#)

Z Li

[The ATLAS Beam Conditions Monitor](#)

V Cindro, D Dobos, I Dolenc et al.

[Laser-Plasma Interaction in Presence of an Obliquely External Magnetic Field: Application to Laser Fusion without Radioactivity](#)

M. Mobaraki and S. Jafari

SiC detector damage and characterization for high intensity laser-plasma diagnostics

L. Torrisi¹ and A. Cannavò

*Dipartimento di Scienze Fisiche-MIFT, Università di Messina,
V.le F.S. d'Alcontres 31, 98166 S. Agata (ME), Italy*

E-mail: lorenzo.torrisi@unime.it

ABSTRACT: Silicon-Carbide (SiC) detectors are always more extensively employed as diagnostics in laser-generated plasma due to their remarkable properties such as their high band gap, high carrier velocity, high detection efficiency, high radiation resistance and low leakage current at room temperature. SiC detectors, in comparison with Si detectors, have the advantage of being insensitive to visible light, having low reverse current at high temperature and high radiation hardness. A similar energy resolution characterizes the two types of detectors, being 0.8% in Si and 1.0% in SiC, as measured detecting 5.8 MeV alpha particles.

Generally, SiC detectors are employed as laser-plasma diagnostics in time-of-flight configuration, permitting the simultaneous detection of photons, electrons and ions based on discrimination of velocity. SiC detectors can be employed in the proportionality regime, because their response is proportional to the radiation energy deposited in the active layer. Using thin absorbers in front of the detectors makes it possible to have further information on the radiation nature, intensity and energy. Surface characterization of SiC before and after prolonged exposure to hot plasma laser generated shows the formation of bulk defects and thin film deposition on the detector surface limiting the device functionality.

KEYWORDS: Detection of defects; Instrumentation and methods for time-of-flight (TOF) spectroscopy; Plasma diagnostics - charged-particle spectroscopy; Solid state detectors

¹Corresponding author.

Contents

1	Introduction	1
2	Experimental set-up	2
3	Results	4
4	Discussion and conclusions	10

1 Introduction

During the last ten years, silicon carbide (SiC) detectors have always been more widely employed as diagnostics in laser-generated plasmas for both low and high laser intensity, high plasma temperature and density, involving laser pulses duration from *ns* to *fs* scales [1]. Their usefulness is due to different advantages in comparison with other semiconductor detectors. The band gap of 3.26 eV does not permit to detect the high intensity of visible light emitted from plasma producing background. The fast charge collection from the thin active areas gives high detection response, indeed, a signal of 100 V is reached in a time of 1 ns. Detection efficiency is generally 100% unless the radiation is absorbed in the thin surface metallization (i.e. at low energies) and when the sensing layer has high transmission due to the thin active layer of the detector (i.e. at high energies). The displacement energy in Si-Si structures of 15 eV [2] is greater than in SiC structures, where the threshold displacement energy is 19 eV and 38 eV for C and Si, respectively [3]. This means that the defects generation threshold in SiC is higher than in Si. In these terms SiC detector has the property of being highly radiation resistant. The low leakage current in SiC, of the order of ten *pA* at room temperature against ten *nA* in Silicon, permits to realize high sensitivity and high temperature resistant detectors [4, 5].

Generally, the use of SiC as diagnostics in laser-generated plasma is performed in time-of-flight (TOF) configuration, because this technique allows the detection of photons, electron and ions emitted from plasma acquired in the same spectrum. The laser-matter interaction, in fact, generates an ionized gas, which expands at supersonic velocity in vacuum emitting photons and particles. Photons are detected almost immediately because the detector generally is placed at a distance less than 1 meter from the target. Since particles are generated at the same energy, in TOF spectroscopy electrons are the first detected particles, followed by protons and heavier ions. TOF are measured using the laser pulse as a start signal and the following arrival time of particles as a stop signal [4]. In TOF applications SiC can be employed also with a thin active layer (5–20 μm in thickness) because the particle energy is evaluated through the flight distance and the arrival time and not from the pulse height generated by the detector. In additional applications, SiC detector can be used in the regime of proportionality between the radiation energy, deposited in the active layer, and the output signal height, due to the charges collected under the electrodes. In this last case

the active layer should be thicker, typically $100\ \mu\text{m}$, in order to collect all the electron-hole pairs produced by high energy ionizing radiations. For example $4\ \text{MeV}$ protons and $15\ \text{MeV}$ alphas can be detected because their range in SiC semiconductor is $99\ \mu\text{m}$ and $90\ \mu\text{m}$, respectively. Generally TOF technique is employed for high radiation fluxes, such as that emitted from sub-nanosecond laser-generated plasmas, while the regime of detector signal proportionality is employed for energy measurements of low fluxes of radiation, such as that emitted from a radioactive ion source.

Using thin absorbers placed in front of the detector it is possible to separate light ions from heavy ones or to separate the energetic particles from those at low energy or to evaluate the X-ray energy from the absorption coefficients of thin films calibrated in thickness [6, 7].

Although SiC detectors are useful for plasma characterization in both single pulse and repetition rate modes and show many advantages with respect to other detectors, their use is limited for these experiments due to the detector damage produced during long-term exposure to plasma in vacuum. Damage consists mainly in crystal defects induced by ions stopped in the active layers, releasing high energy at the Bragg peak, and in the coating and contamination of their surface due to clusters, debris, molecules and atoms generated by both plasma and secondary radiations in the vacuum chamber where the plasma is produced. The damage of SiC detectors as a function of the ion flux exposure time and the number of plasma exposures at intensity laser of the order of $10^{15}\ \text{W}/\text{cm}^2$ will be presented and discussed.

2 Experimental set-up

In these measurements 4H-SiC Schottky diode detectors were employed and, for comparison, a silicon surface barrier (SSB) detector. Figure 1a shows the theoretical detection efficiency, in terms of results of the simulation interaction probability of radiation stopped in the active volume of the detector, as a function of the radiation energy. The simulations were obtained for a SiC detector with $200\ \text{nm}$ Ni_2Si surface metallization, an active region $80\ \mu\text{m}$ thick of 4H-SiC n-doped at $10^{14}\ \text{cm}^{-3}$ and a 4H-SiC substrate, $220\ \mu\text{m}$ thick, highly doped and metallized with ohmic contact. The active region depth of the detector depends on the reverse bias applied to the SiC Schottky barrier in vacuum. Its growth is roughly linear with the applied reverse voltage assuming a value of about $10\ \mu\text{m}/100\ \text{V}$ up to a maximum value of $80\ \mu\text{m}/800\ \text{V}$, at which value the active region saturates, as reported in a previous contribution [8]. Figure 1b and 1c show a schematic of the detector geometry and a picture, respectively. Figure 1d shows the theoretical detection efficiency, in terms of simulated interaction probability, of a Si-SSB detector with $20\ \text{nm}$ Au surface metallization, an active region $100\ \mu\text{m}$ thickness with n-doping at $10^{13}\ \text{cm}^{-3}$ and a Si substrate $200\ \mu\text{m}$ thick at high doping, back ohmic metallized. The SSB-Ortec detector needs $+50\ \text{V}$ reverse polarization to produce a depletion layer $100\ \mu\text{m}$ wide [9].

Figure 1e and 1f show a scheme of the detector geometry and a picture respectively. The active surface of the SiC and Si detectors are $2\ \text{mm}^2$ and $50\ \text{mm}^2$, respectively.

The reported detection efficiencies in figure 1a, in terms of interaction probability, were calculated using simulation codes, such as SRIM [10] for ions, CXRO [11] web database for X-rays and ESTAR [12] for electrons. These plots report the theoretical ratio between the energy lost by the radiation in the active region of the detector and the total incident energy, for different kind of radiation (X-rays, electrons, protons and alpha particles). The efficiency at low energy is strongly

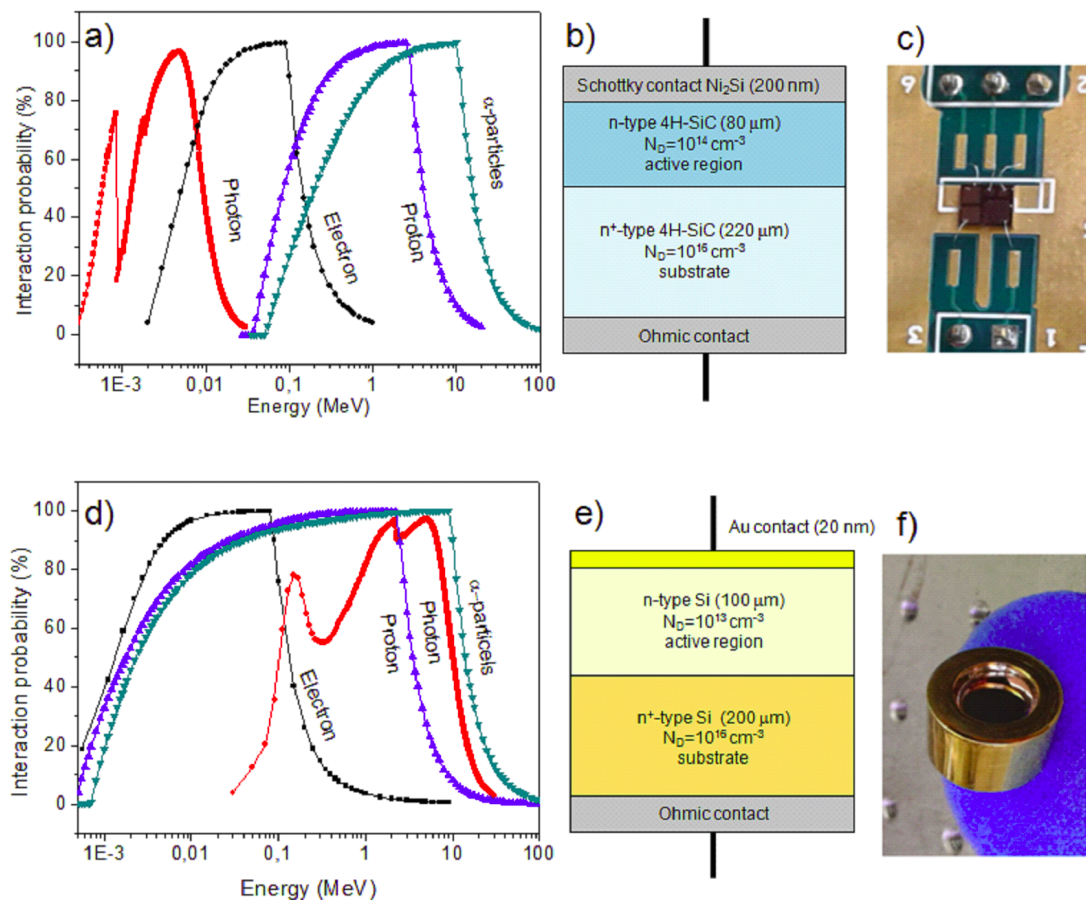


Figure 1. Interaction probability (simulation of detection efficiency) of SiC (a), scheme of the SiC structure (b) and a picture of the SiC detector (c); comparison with Si-SSB interaction probability (d), scheme of Si structure (e) and a picture of the Si detector (f).

influenced by the thickness of the surface metallization layer, absorbing all low energy particles having a range lower than its thickness. At high energy the efficiency decreases due to the limited active layer thickness that can be crossed by the radiation with a minimum energy release.

Measurements of detector energy resolution were obtained using electronics based on: a preamplifier (Ortec mod. 142 A) at 45 mV/MeV, a linear amplifier (Ortec mod. 672) with 10 μ s shaping time and 50 coarse gain, a very compact digital Multi Channel Analyzer (Amptek MCA-8000D) to digitize the analogical input signal and a PC interfaced with DPPMCA software to acquire the spectra. A multi-peak alpha source was employed for energy resolution measurements. It contains ^{241}Am , ^{244}Cm and ^{239}Pu with activity of 774.40 Bq, 255.88 Bq and 1058.80 Bq, respectively. The alpha mean energy is 5.498 MeV, 5.818 MeV and 5.164 MeV for ^{241}Am , ^{244}Cm and ^{239}Pu , respectively. The alpha source was placed in front of the detector at 6 mm distant from its surface, in high vacuum conditions (10^{-5} mbar).

I–V measurements in SiC were performed in high vacuum and different bias, from -100 up to -600 V using a precision Keithley picoammeter.

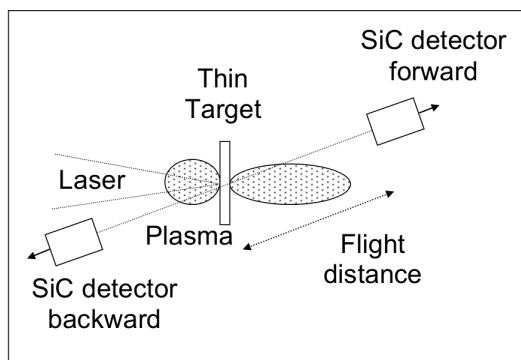


Figure 2. Scheme of the experimental set-up employed for the TNSA measurements at PALS laboratory using forward and backward SiC detectors in TOF approach.

SiC detectors, used in TOF approach, were exposed to laser-generated plasma in the PALS laboratory, in Prague (Czech Republic) [8]. The iodine laser characteristics were 600 J pulse energy, 1315 nm wavelength, 300 ps pulse energy, 5×10^{15} W/cm² average laser intensity and single pulse mode. Generally the SiC detectors were employed at a distance of 80 cm (flight distance) from the laser irradiated target, at which plasma is created, and at an angle of 30° with respect to the normal to the target surface, in both forward and backward directions, as shown in the schematic of figure 2. For plasma investigations SiC detectors were employed in high vacuum (10^{-5} mbar) with a bias polarization of 800 V at which the depletion layer is about 80 μ m. SiC were polarized through 1 M Ω resistor and coupled to a fast storage oscilloscope (Tektronix, high bandwidth, 20 GS/s) using 1 μ F capacitance. Laser irradiated targets were thin polymeric foils (polyethylene, mylar and PMMA), pure Au foils (from 1 μ m up to 30 μ m) and polymers covered with Au thin films (10–100 nm thickness). The laser light incidence angle was 0° and the SiC were used in target-normal-sheath-acceleration (TNSA) regime, in order to have high ion acceleration. Such experiments permit to generate non-equilibrium plasma in which the charge separations generate very high electric fields producing high ion acceleration, as described in the previous papers [13, 14].

Optical and electronic microscopy investigation was used to observe the surface of the SiC detector at different plasma exposure times in PALS laboratory.

3 Results

Figure 3 shows a comparison between the experimental spectra for the detection of alpha particles from the calibrated radioactive source using SiC (a) and Si-SSB (b) detectors. The SiC detector was polarized with -300 V and Si detector with + 50 V, the electronics was the same. At 300 V the active region is 30 microns deep, sufficient to stop 5.8 MeV alpha particles that have a range in SiC of 20 microns.

Due to the different detector geometries the detection solid angle was of 30 msr for Si detector and of 0.3 msr for SiC. The theoretical detection efficiency for 5 MeV alpha particles was about 100% for both detectors. Thus, in order to obtain comparable yields, the acquisition time was 300 s for Si detector and 3000 s for the SiC detector. The spectra are characterized by three broad structures that, in order to determine the energy resolution, were fitted using Gaussian functions. The FWHM

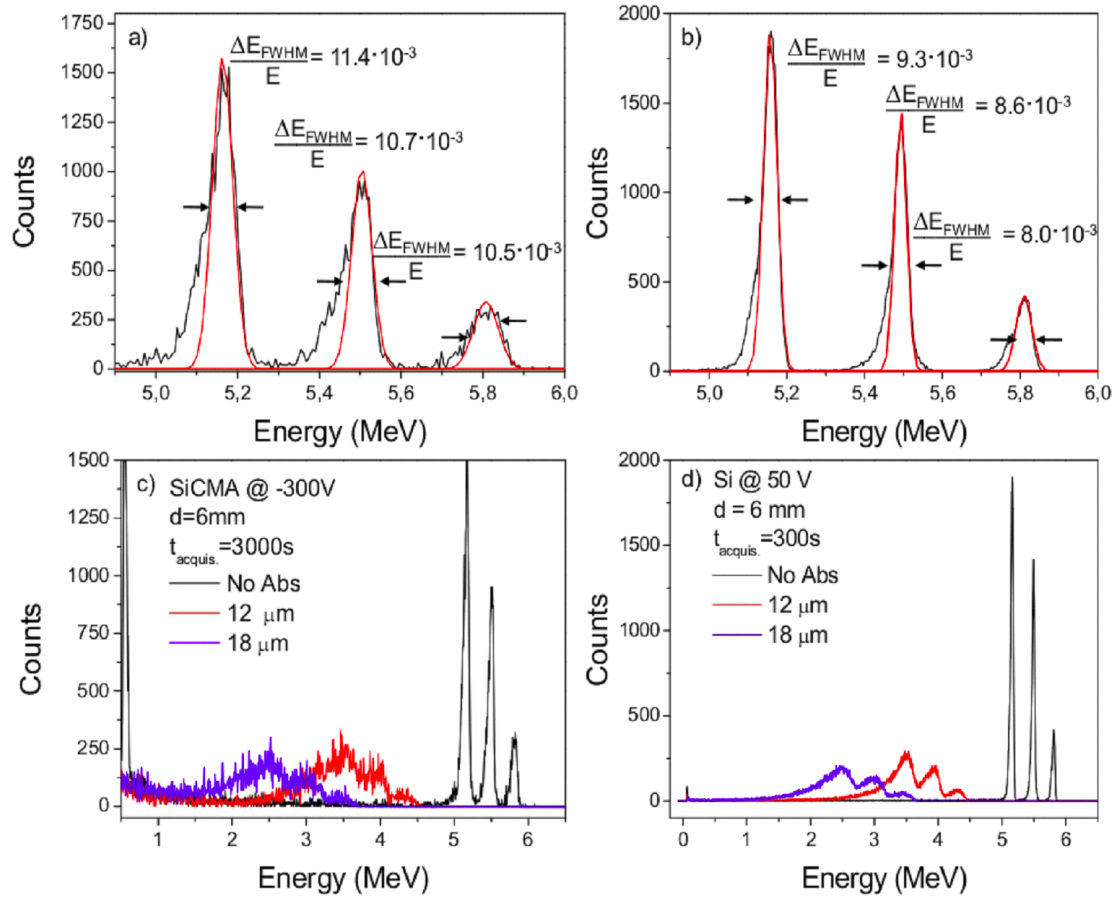


Figure 3. Three peaks alpha spectra detected using SiC (a) and Si-SSB (b) for energy resolution measurements without absorbers and comparison with 12 μm and 18 μm thickness mylar absorbers, for SiC (c) and for Si (d), respectively.

(Full Width Half Maximum) energy, ΔE_{FWHM} , and the exact value of the centroid-peak energy, E , were employed to calculate the percentage energy resolution R in terms of $R = (\Delta E_{\text{FWHM}} \times 100)/E$. The energy resolution at 5.8 MeV alpha particles is 0.8% in Si and 1.05% in SiC.

A thin foil of mylar, 6 μm , 12 μm and 18 μm thick, was placed in front of the radioactive source to reduce the alpha energy and to evaluate the spectra at lower alpha particle energies for the SiC and Si detectors in the presence of a strong energy straggling absorber. Figure 2c and figure 2d shows alpha spectra comparisons of SiC and Si detectors without absorber and with thin mylar foils of 12 μm and 18 μm , respectively. The spectrum with 6 micron filter has not been presented because there was no significant difference with respect to the spectrum achieved without absorber; in fact the alpha energy loss in this thin absorber was only 400 keV.

Figure 4 shows the comparison of the energy resolution measurements performed in SiC and Si-SSB detectors, the first with -300 V bias and the second at +50 V, using the same electronics. Although the Si detector shows resolution values of 20% lower than SiC, the resolutions vs. alpha particle energy for both these two detectors are similar. The Si extra data points at alpha energies between 3.5 and 5 MeV comes from the Ortec literature [15].

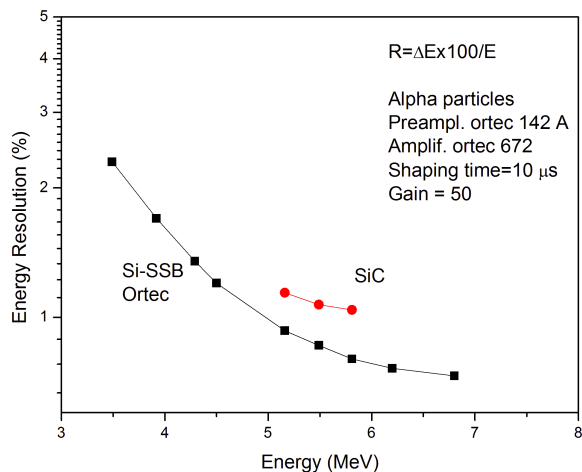


Figure 4. Energy resolution (%) as a function of alpha energy for Si-SSB and for SiC using the same detection electronics.

Using thin mylar absorbers placed in front of the detectors it was possible to reduce the mean alpha energy due to their energy loss in the absorber. Although the alpha energy straggling in the absorbers causes an increment of the resolution value, because spectra peaks enlarge, the comparison between SiC and Si energy resolutions continues to appear similar.

Figure 5a shows the result of the I-V measurements obtained reverse biasing the SiC Schottky junction and monitoring the leakage current with different bias values and at room temperature (21°C). The figure reports the I-V curves comparison of 14 SiC detectors, from SiC1 to SiC14, exposed for different times to the laser-generated plasma. It is possible to observe that the inverse current at 100 V reverse bias ranges between about 10 pA for un-exposed detectors (new SiCs) up to about 10 nA for high used SiCs and extending up to about 100–1000 nA for high damaged detectors exposed to many times (about 400) to plasma pulses. For comparison the plot shows also the typical reverse current of Si-SSB detectors (Si A and Si B). Figure 5b reports the dependence of the inverse current in three SiC detectors, evaluated at -300 V applied bias, as a function of the number of exposures to the plasma generated by PALS laser operating in a single pulse mode, 300 ps duration and intensity $5 \times 10^{15} \text{ W/cm}^2$. The detectors are generally placed at 80 cm distance from the target and at 30° angle with respect to the target normal forward direction, during target-normal-sheath-acceleration (TNSA) regime experiments [13, 14]. In these measurements the laser has irradiated targets containing hydrogenated polymers and metals. Generally the ion acceleration was higher than 1 MeV per charge state. Plasma produced by polymers is rich in carbon ions that, being ionized up to 6+ charge states, have Boltzmann energy distributions extended from about ten keV up to more than 6 MeV kinetic energy [13]. Heavy metals and gold ions in plasma show high charge states, up to about 60+, and broader energy distributions, from some keV up to values above 60 MeV, as reported in the literature [14]. From the semi-logarithmic plot of figure 5b it is possible to observe that the inverse SiC current growth is approximately exponential with respect to the number of plasma exposures. The effect of leakage current increment with the exposure times is due to the

defects generated in the active layer by the high LET (linear energy transfer) radiation. Mainly energetic heavy ions, such as gold, having high nuclear stopping power may produce collision cascades with Si and C atoms moving from their equilibrium positions and generating defects, such as vacancies, interstitial and others. Such generated defects reduce the electron-hole mobility enhancing the diode leakage current.

Literature reports that SiC can be amorphized by high doses at the Bragg peak positions producing extended defects, while localized point defects can be induced at low ion doses [16]. The most common types of defects can be vacancies, interstitial atoms, Frenkel pairs generated by displacement cascades and amorphization zones during further accumulation of defects [17]. Generally the defects generation depends on the implanted dose, however, it is difficult to evaluate with accuracy the dose received by the SiC during the laser-generated plasma, because different plasma characteristics (temperature, density, energy and charge state distributions, . . .) were adopted in several experiments. Based on RBS (Rutherford backscattering spectrometry) analysis of ion implanted Si-substrates placed near to the SiC detectors, approximated evaluations indicate that ion doses of the order of 10^{14} ions/cm² are absorbed for each laser shot at PALS, as reported in the literature [18]. Moreover, because at these laser intensities the ion energy distributions follow a Coulomb-Boltzmann-shifted function [19], i.e. because the different charge states have different kinetic energy and range in the detector, the defects are not well localized in the detector but should be distributed approximately uniformly in the entire active zone.

In addition to the generated crystallographic defects in the active volume by high LET ions, another type of defect is caused on SiC exposed to laser-generated plasma. It consists in the coating and contamination of the surface by debris constituted by micrometric and nanometric clusters, molecules and atoms deposited from plasma. The plasma exposure time enhances the thickness of such deposited film, whose composition depends on the nature of the laser irradiated target, plasma properties (temperature, density, angular distribution of emitted particles, . . .) and geometrical position of the SiC detector with respect to the target. The film morphology depends on the laser irradiated target material, plasma and laser properties. Laser wavelength and intensity, in facts, influence the photothermal (IR) and photochemical (UV) ablation regimes giving rise to more atomic species or molecular or cluster emission during plasma production [20].

The charge separation effects in the TNSA regime produces high electric fields accelerating ions mainly along the normal direction in both forward and backward directions [21]. Such energetic ions, which kinetic energy decreases at large angles with respect to the normal direction, can be implanted in the SiC surface enhancing the adhesion of the film deposited on the surface.

Generally the surface coverage is not uniform because nanometric and micrometric clusters are not emitted isotropically from the plasma, giving rise to localized debris randomly distributed masking the total area of the exposed detector. Figure 6 shows a set of four optical microscope images of the SiC detector surfaces exposed for different times to the laser-generated plasma at the PALS facility. The images show micrometric debris deposited on the detector surface, together with vapors coming from the laser-generated plasma. The reported figures are related to a different number of plasma exposures of SiC, from a minimum number of 20 (d), to 100 (c), to 300 (b), up to a maximum number of plasma exposures of about 400 (a). An image treatment software permitted to evaluate the number of particles and their size distribution as a function of the plasma exposures from PALS measurements, as reported in figure 6 a', b', c' and d', relative to 400, 300, 100 and 20

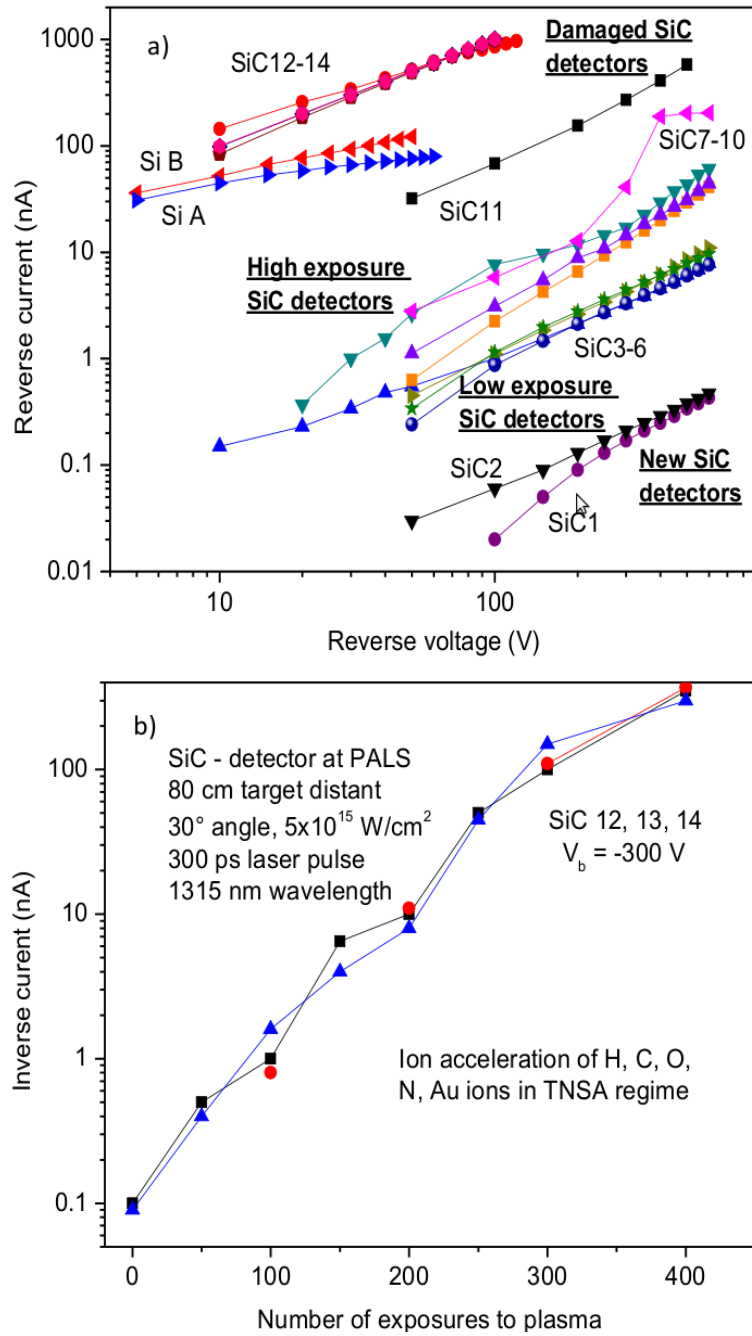


Figure 5. Leakage current versus voltage for 14 SiC detectors exposed for different times to the laser-generated plasma at PALS facility and comparison with Si detectors (a) and reverse current in 3 SiCs as a function of the number of plasma exposures (b).

plasma exposures, respectively. Figure 6 is relative to detectors, used during TNSA regime of ion acceleration experiments, placed at 80–60 cm far from the target in the forward and backward at 30° and 150° angles, with respect to the target normal direction.

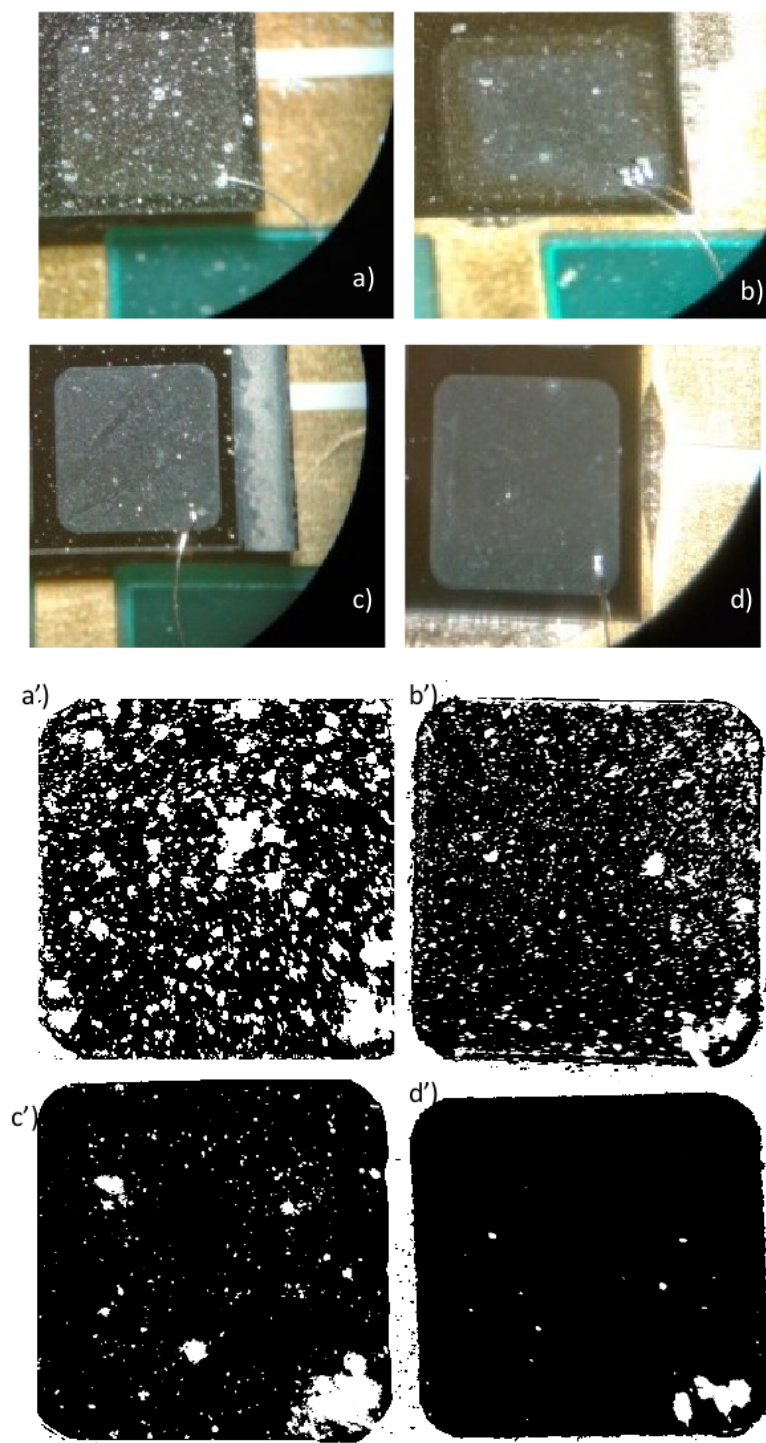


Figure 6. Optical microscope photographs of the SiC surfaces exposed to the laser-generated plasma at PALS about 400 times (a), 300 times (b), 150 times (c) and 20 times (d) and image treatment to evince the grain size distributions (a'), (b'), (c') and (d'), respectively.

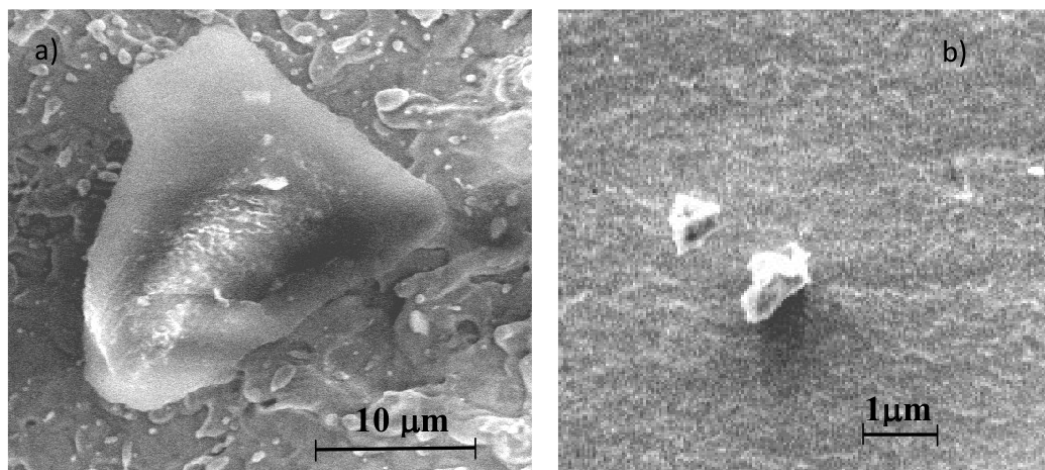


Figure 7. SEM pictures of typical debris deposited on the SiC surface with a dimension of tens microns (a) and of about 1 micron (b).

Optical and electronic (SEM) microscope investigations indicate that the deposited debris have a large size distribution with an average value of about 10–30 microns and that also submicrometric clusters with dimensions from 10 nm up to about 1 micron are present, as shown by the SEM pictures of figure 7a and 7b, respectively. This thin and non-uniform surface coating and contamination of the detector produces attenuation of the incident radiation, energy loss of the detected particles and decreasing of the detector signal due to the lower free exposed surface. 10 MeV alpha particles, for example, can be fully stopped in 22 μm gold clusters because their range is 21.6 μm . Also heavier ions cannot be detected because of absorption in the thick layer of debris. Gold ions, for example, should have energy higher than 100 MeV to cross a gold debris thickness of 10 μm and in this case protons should have an energy higher than 1.5 MeV to be detected.

The decrement of SiC exposed surface due to micrometric debris deposition produces a reduction of the free useful surface and consequently a reduction of the detector signal, as demonstrated by our investigations analyzing alpha particles emitted from a radioactive source and using SiCs with different free active areas due to coverage by many micrometric clusters. Figure 8a shows a SiC spectra comparison related to the three peak alpha source detected using a new detector, which surface is 100% free by debris (a), and a SiC detector which surface is debris-free in percentages of 53.2% (b) and 24.8% (c). The corresponding SiC signal, observed in the multichannel analyzer spectrum as count yield, has a linear decrement proportional to the exposed area. The plot in figure 8b, reporting the peak yield (maximum peak counts) versus the exposed area (%), demonstrates that, for alpha particles with a mean kinetic energy of about 5 MeV, the detector signal growth is proportional to the exposed active area, free from micrometric debris and deposited clusters.

4 Discussion and conclusions

This presentation shows that SiC energy resolution is comparable to that of Si-SSB Ortec detectors, showing a decrease of about 20% with respect to Si, as evaluated at 5.8 MeV alpha particles. SiC detectors can be employed with success in the regime of signal proportionality to the energy released

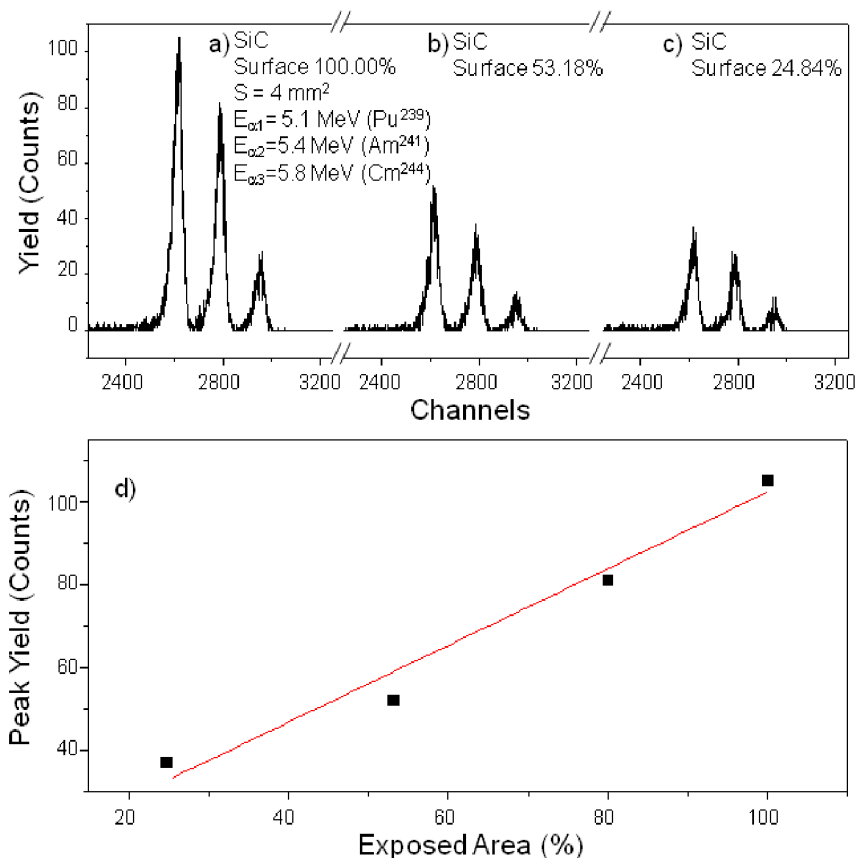


Figure 8. Three peaks alpha spectra detected with a SiC with debris-free surface in 100% (a), 53.18% (b) and 24.84% (c) and peak yield (counts at the peak) vs. exposed area (d).

by the radiation in the depletion layer and converted to electron-hole pairs. However, in the field of laser-generated plasma SiC detectors are generally employed in TOF regime to evaluate the particle energy from the flight distance and arrival time at the detector using the laser light as start signal. In this case, also if the SiC signal is low and not proportional to the energy carried by the particles, but above the detection threshold (leakage current), it is possible to evaluate the particle energy accurately from the TOF measure [13]. SiC have two big advantages with respect to Si detectors, the first due to the higher gap of 3.26 eV, compared to 1.1 eV for Si, which does not allow to detect the high visible light intensity produced by plasma developing high visible background and the second due to the lower reverse current at room temperature, about three orders of magnitude less than silicon.

Although the SiC surface is very little, only $2 \times 2 \text{ mm}$, and the subtended solid angle is of the order of 0.3 msr, the SiC signal may reach values of the order of ten of volts, due to the high radiation flux from the plasma, permitting significant information to be gathered on the plasma properties in terms of emitted photons, electrons and ions, ion kinetic energy, plasma temperature and density.

Moreover, the present research has highlighted some aspects concerning the damage caused in SiC detectors when exposed for long times to laser-generated plasmas. Results are presented on

measurements carried out at the PALS facility using an Iodine laser operating at 1315 nm, 300 ps pulse duration, 5×10^{15} W/cm² intensity, irradiating thin foils in the TNSA regime and positioning the SiC detectors at 80–60 cm distance from the targets and at 30° angle with respect to the target normal direction. Two types of main damage were encountered in the SiC when many plasma exposures occur.

The first is localized in the bulk, and more specifically in the active region. It consists in the defects mainly due to the high nuclear stopping power of ions that produce collision cascades and atom displacements with crystal amorphization at high ion dose. The high intensity of photons, electrons and ions may produce high ionization density along the ion and delta ray tracks and induce localized and extended defects. The accumulation of defect centers with the absorbed dose increases the leakage current in the diode worsening its sensitivity and energy resolution. To remove these defects a thermal annealing may be employed, but this produces atom diffusion and deterioration of the active junction, thus it is not applicable.

The second kind of defect concerns the detector surface which is covered by evaporated and ablated material from the target and, overall, by micrometric debris deposition from the target during plasma production. Gradually the useful surface of the detector is reduced by the deposit of large micrometric particles decreasing the useful electric signal. Exposing to high doses the active area results completely covered producing a signal decreases to the background value and rendering the detector unusable. This damage could be eliminated using thin foils placed in front of the detector which are successively removed and replaced after dozens plasma exposures, as we have already tested in previous experiments using thin absorbers to filter the more energetic ions [6]. Of course the grain dimensions of the order of 10–30 μm absorb ions and generate ion energy loss modifying the efficiency of the detector with the absorbed dose.

Assuming that an average dose of about 10^{14} ions/cm² is produced by a single plasma exposure, our measurements indicated that the investigated defects occur for the detector exposures to about 100 plasma pulses, i.e. to an ion dose exposure of the order of 10^{16} ions/cm².

Acknowledgments

The authors thank Laserlab-Europe supporting this research (project PALS 001823, N. 108/12/G108).

Also, many thanks also to the PALS laboratory for the use of laser facility and technical support given to this experiment.

References

- [1] L. Torrioni et al., *Proton emission from thin hydrogenated targets irradiated by laser pulses at 10^{16} W/cm²*, *Rev. Sci. Instrum.* **83** (2012) 02B315.
- [2] J.F. Zeigler, J.P. Biersack and U. Littmark, *The Stopping and Range of Ions in Solids*, Pergamon Press, New York U.S.A. (1985).
- [3] G. Lucas and L. Pizzagalli, *Ab initio molecular dynamics calculations of threshold displacement energies in silicon carbide*, *Phys. Rev.* **B 72** (2005) 161202.
- [4] M. Cutroneo et al., *High performance SiC detectors for MeV ion beams generated by intense pulsed laser plasmas*, *J. Mater. Res.* **28** (2012) 87.

- [5] A. Testa, S. De Caro, S. Russo, D. Patti and L. Torrisi, *High temperature long term stability of SiC Schottky diodes*, *Microelectron. Reliab.* **51** (2011) 1778.
- [6] L. Torrisi et al., *Proton driven acceleration by intense laser pulses irradiating thin hydrogenated targets*, *Appl. Surf. Sci.* **272** (2013) 2.
- [7] L. Torrisi and E. Amato, *X-ray emission from plasma generated by nanosecond laser irradiating tantalum*, *Radiat. Eff. Def. S.* **160** (2005) 391.
- [8] L. Torrisi et al., *Single crystal silicon carbide detector of emitted ions and soft x-rays from power laser-generated plasmas*, *J. Appl. Phys.* **105** (2009) 123304.
- [9] EG&G Ortec, *Review of Physics of semiconductor detectors*, *Ortec databook*, actual website: www.ortec-online.com/download/ORTEC-Catalog-Detectors-Section.pdf.
- [10] J. Ziegler, *SRIM-The Stopping and range of Ions in Matter*, actual website (2016): <http://www.srim.org/>.
- [11] Berkeley Lab, *CXRO-X-Ray interaction with Matter*, actual website (2016): http://henke.lbl.gov/optical_constants/.
- [12] NIST-ESTAR — *Stopping power and range tables for electrons*, actual website (2016): <http://physics.nist.gov/PhysRefData/Star/Text/ESTAR.html>.
- [13] L. Torrisi, *Ion energy enhancement from TNSA plasmas obtained from advanced targets*, *Laser Part. Beams* **32** (2014) 383.
- [14] L. Torrisi, L. Calcagno, D. Giulietti, M. Cutroneo, M. Zimbone and J. Skala, *Laser irradiations of advanced targets promoting absorption resonance for ion acceleration in TNSA regime*, *Nucl. Instrum. Meth. B* **355** (2015) 221.
- [15] EG&G Ortec, *Alpha spectroscopy with surface barrier detectors*, *Experiment n.4*, 25-31 Ortec databook, in actual web site (2016): <http://physicsweb.phy.uic.edu/482/Alpha/AN34-Exp04.pdf>.
- [16] A. Declémy et al., *An IR-reflectivity and X-ray diffraction study of high energy He-ion implantation-induced damage in 4H-SiC*, *Nucl. Instrum. Meth. B* **186** (2002) 318.
- [17] T. Diaz de la Rubia and G.H. Gilmer, *Structural Transformations and Defect Production in Ion Implanted Silicon: A Molecular Dynamics Simulation Study*, *Phys. Rev. Lett.* **74** (1995) 2507.
- [18] M. Cutroneo et al., *Ta-ion implantation induced by a high-intensity laser for plasma diagnostics and target preparation*, *Nucl. Instrum. Meth. B* **365** (2015) 384.
- [19] L. Torrisi, *Coulomb-Boltzmann-Shifted (CBS) distribution in laser-generated plasmas from 10^{10} up to 10^{19} W/cm² intensities*, *Radiat. Eff. Defect. S.* **171** (2016) 34.
- [20] L. Torrisi, A. Borrielli and D. Margarone, *Study on the ablation threshold induced by pulsed lasers at different wavelengths*, *Nucl. Instrum. Meth. B* **255** (2007) 373.
- [21] L. Torrisi, *Ion acceleration from intense laser-generated plasma: methods, diagnostics and possible applications*, *Nukleonika* **60** (2015) 207.